Damage Evolution in Flexible Polyurethane Foams

C. KAU,[1] L. HUBER,[2] A. HILTNER,[1] and E. BAER[1,*]

[1]Department of Macromolecular Science, Case Western Reserve University, Cleveland, Ohio 44106;
[2]The Dow Chemical Company, Freeport, Texas 77540

SYNOPSIS

Microcrazing in the struts of flexible polyurethane foams was discovered during compressive deformation and observed directly in the scanning electron microscope. Attributed to this phenomena was the decrease in stress at maximum compression and the intensity of acoustic emission during compressive cycling. The higher content of styrene–acrylonitrile (SAN) copolymer in these foams resulted in higher modulus, more severe microcrazing, an increase in acoustic emission activity, and a decrease in the stress at maximum compression as cycling progressed.

INTRODUCTION

Basically, there are two interrelated approaches for the investigation of foamed polymers. The physical approach is an attempt to correlate the macroscopic properties to morphological parameters such as density and cell size,[1-10] whereas the chemical approach attempts to explain and predict foam behavior from the chemical composition and the process history of the polymer foam.[11-14] In general, it can be concluded that properties of urethane polymers in cellular applications are primarily related to the cell structure and the properties of the base polymer.

For successful utility of flexible polyurethane (PU) foams, the load-bearing properties and the dynamic fatigue resistance are important performance requirements. When a flexible PU foam is subjected to cyclic compressive deformation, it is found that the initial elastic modulus and the overall load-bearing capacity decrease with an increasing number of deformation cycles. The change in the mechanical properties is largest for the first and second compressions and steady-state values of the properties are usually obtained after a small number of cycles.[15-17] Most previous investigators hypothesized that the reduction of load-bearing capacity is due to molecular effects such as the rearrangement of the hydrogen bonding between the macromolecular chains of the urethane material and attempted to confirm their hypothesis by usually changing the ingredients in the foam formulation.[18-21]

Although many attempts to correlate the fatigue performance in PU foams have been made through chemical modification, direct observation of damage mechanisms and damage progression during fatigue loading has not been widely investigated. Lee[22] reported the rupture of cell struts after fatigue loading at low magnifications. However, direct observations of changes in morphological structure at the microscale during compressive loading and how these irreversible processes relate to fatigue performance of flexible PU foams has not been studied. Two techniques have been used extensively in determining real-time damage progression and for the identification of damage mechanisms by Baer, Hiltner, and coauthors[23-26] in other heterogeneous polymeric systems. Scanning electron microscopy was applied to reveal the microscopic damage mechanisms and acoustic emission (AE) was utilized to detect the energy dissipation spectrum when the material fails.

In this paper, we demonstrate the applicability of these techniques to identify the extent of damage

* To whom correspondence should be addressed.

Journal of Applied Polymer Science, Vol. 44, 2069–2079 (1992)
 CCC 0021-8995/92/122069-11$04.00

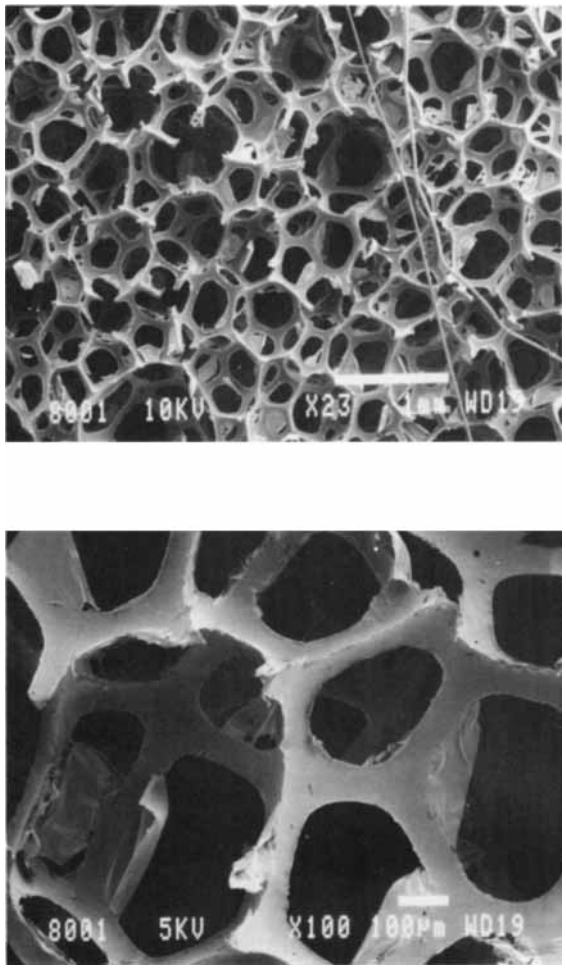

Figure 1 SEM photographs show 3-dimensional polyhedral cellular structure of flexible PU foam. Cell struts shown in higher magnification are the major load-bearing component in the foam structure.

evolution and the irreversible damage mechanisms in flexible PU foams during compressive cycling. The results obtained from AE monitoring were confirmed by direct observations in the SEM in order to obtain relations between the extent of microcrazing, the amount of AE activity, and the loss in load-bearing capacity.

II. EXPERIMENTAL

1. Materials

The materials used in this study were flexible PU foams, generously supplied by the Dow Chemical Company. Figure 1 shows the 3-dimensional polyhedral cellular structure of a foam sample. The struts, shown in a higher magnification, are the major load-bearing components. These foams were made by combining Dow's Varanol 3137 polyol and Varanol 3943 copolymer polyol, which contains 43% by weight of a finely dispersed styrene–acrylonitrile (SAN) copolymer. The average diameter of the SAN particles ranged between 2000 and 3000 Å. The modulus and plateau stress increases with increasing SAN copolymer particle concentration. The compositions and mechanical properties of these foams are listed in Table I.

2. Mechanical Properties Measurements with Acoustic Emission (AE) Monitoring

Rectangular block specimens, $100 \times 100 \times 50$ mm^3, were cut parallel to the foam rise direction from foam buns. Cyclic compressive tests were carried out at room temperature at a strain rate of 40% min^{-1} using an Instron mechanical testing machine. A specially designed fixture of essentially two parallel discs with AE sensors embedded in the center as illustrated in Figure 2 were used.

During a test, foam samples were first loaded to 75% compression and unloaded to 55% compression at the same rate. This cycle was repeated between these two compression ratios for 1000 times. Changes of the load-bearing capacity (the stress at maximum compression) was recorded throughout these tests. The AE dissipation due to damage evolution in the foam sample during this cyclic compression was monitored by a PAC 4003 AE system made by the Physical Acoustic Corporation.

3. Compressive Cycling in SEM

A foam specimen of $10 \times 10 \times 10$ mm^3 was placed under compression in a modified SEM stage (Fig. 3), which allows compressive loading by simply turning a screw manually to the desired strains. The cyclic loading conditions previously conducted in the Instron were simulated in this SEM experiment. Before loading, the samples were lightly coated (30 Å) gold–palladium. SEM photographs of the struts were taken before straining and at 75% compression of the first cycle. Also, samples that had been loaded cyclicly between 75 and 55% compression ratios for 50 times were observed on the 51st cycle at 75% compression.

Table I The Composition and Mechanical Properties of PU Flexible Foams under Compression ($\times 10^{-3}$)

	Foam			
	A	B	C	D
Voranol 3137[a]	100	75	50	0
Voranol 3943[a]	0	25	50	100
Density, g/cm^3	0.026	0.025	0.025	0.026
Modulus (MPa)[b]	97	190	200	410
Yield stress (MPa)	6.0	8.4	9.8	24

[a] Trademark of the Dow Chemical Company. Voranol 3139: pure polyol. Voranol 3943: SAN copolymer polyol.
[b] Modulus = (load/cross-sectional area)/(compression distance/original thickness).

III. RESULTS AND DISCUSSION

1. Compressive Cyclic Loading

The compressive stress–strain and cyclic loading behavior between 75 and 55% strains in compression of foam C (50% SAN copolymer) and foam D (100% SAN copolymer) are illustrated in Figure 4. Three regions can be differentiated from these curves. In region I, where the foam cell strut joints bend, the material exhibits a nominal Hookean behavior. A yield zone followed by a plateau region is identified as region II, where buckling of struts occurs. In region III, the densification of cell struts gives a sharp increase in the stress. Higher SAN copolymer content results in a higher modulus as well as a higher plateau stress (Table I). In both foams, the stress at maximum compression of each cycle decreased rapidly in the early stage of cycling and then gradually leveled off as cycling progressed. Figure 5(a) shows the decay of the stress at maximum compression vs. the number of cycles comparing both foams. To compare the decrease of stress at maximum compression for both foams [Fig. 5(a)], these curves were normalized by taking the ratio of the stress drop to the maximum stress of the first cycle as

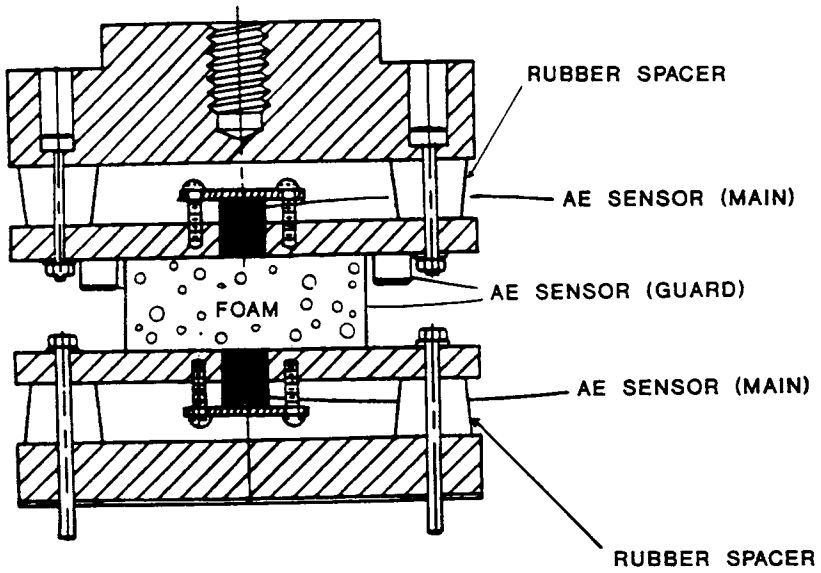

Figure 2 Apparatus for compressive cyclic loading with AE monitoring. Two parallel discs with AE sensor embedded in the center are designed to detect the AE signal from foam specimen during cyclic loading.

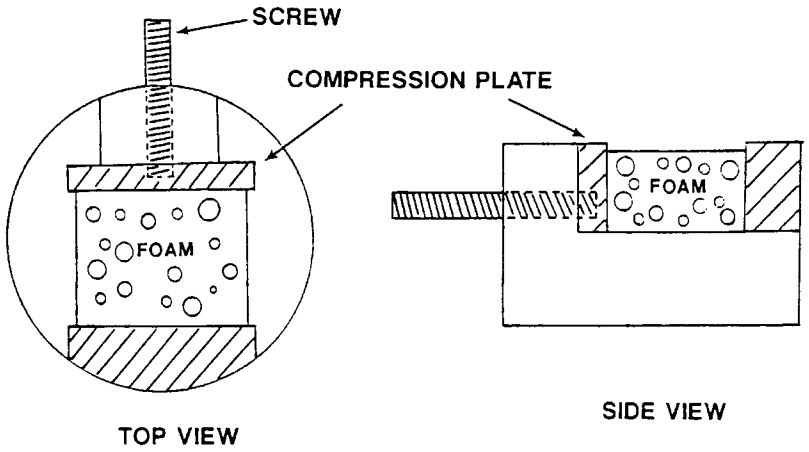

Figure 3 A modified SEM stage for compressive deformation.

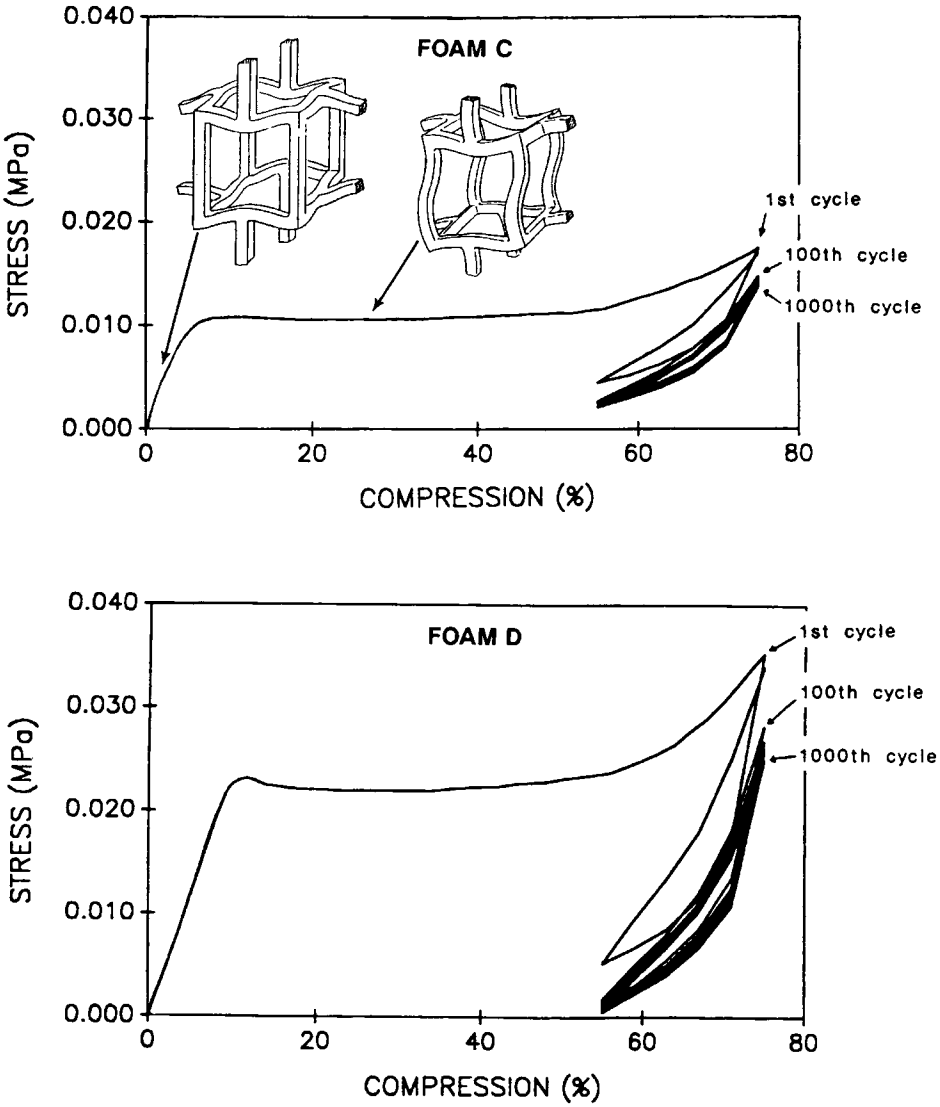

Figure 4 Compressive stress–strain curves and fatigue-loading loops from 75 to 55% compressive strains of foams C and D.

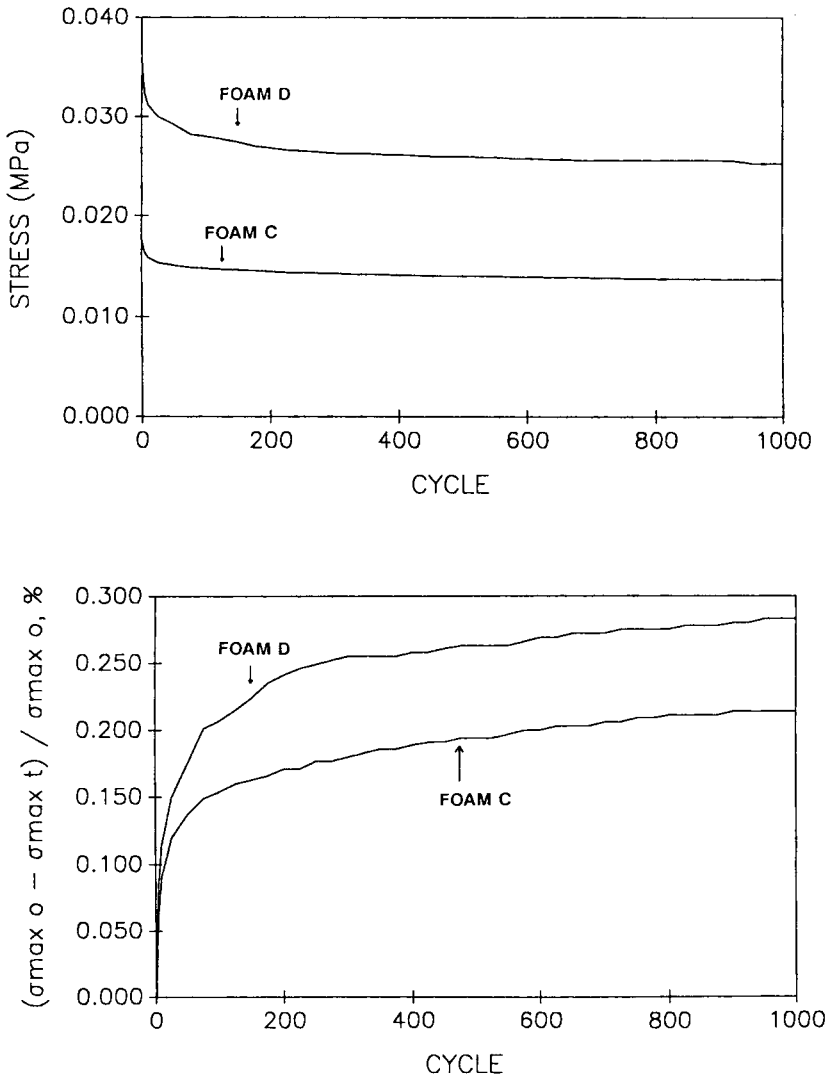

Figure 5 (a) Stresses at maximum compression vs. cycles of foams C and D. (b) Normalized stress vs. cycles curves of foams C and D. σ_0: stress at maximum compression of first cycle; σ_t: stress at maximum compression of subsequent cycles.

shown in Figure 5(b). Foam D, which has twice the amount of SAN copolymer than foam C, shows more stress decay in the first 300 cycles than does foam C. Subsequently, both foams are similar, indicating that foam D was subjected to more severe damage than was foam C in the early cycles. It has been previously reported by several authors[19-22] that in the early stage of cycling a sharp decrease in the load-bearing capacity of flexible PU foams is due mainly to the breakage of hydrogen bonds between molecules. In the present study, the continuous decrease of stress at maximum strain up to 300 cycles suggests that damage processes other than hydrogen-bond failure could be involved.

The AE technique, which detects energy dissipation resulting from irreversible deformation, was applied to monitor the damage progression during foam fatigue. Figure 6 illustrates the AE activity of foams C and D during the first 30 cycles. Each dot represents one acoustic event at the corresponding stress level where the damage occurred. In both systems, the AE events that occurred in the first cycle are probably due to the breakage of windows. However, foams C and D are different. Foam D shows a pattern of AE activity after the fifth cycle during the highest cyclic stress levels. This observation indicates that as cycling continued considerable damage occurred periodically in foam D, while less dam-

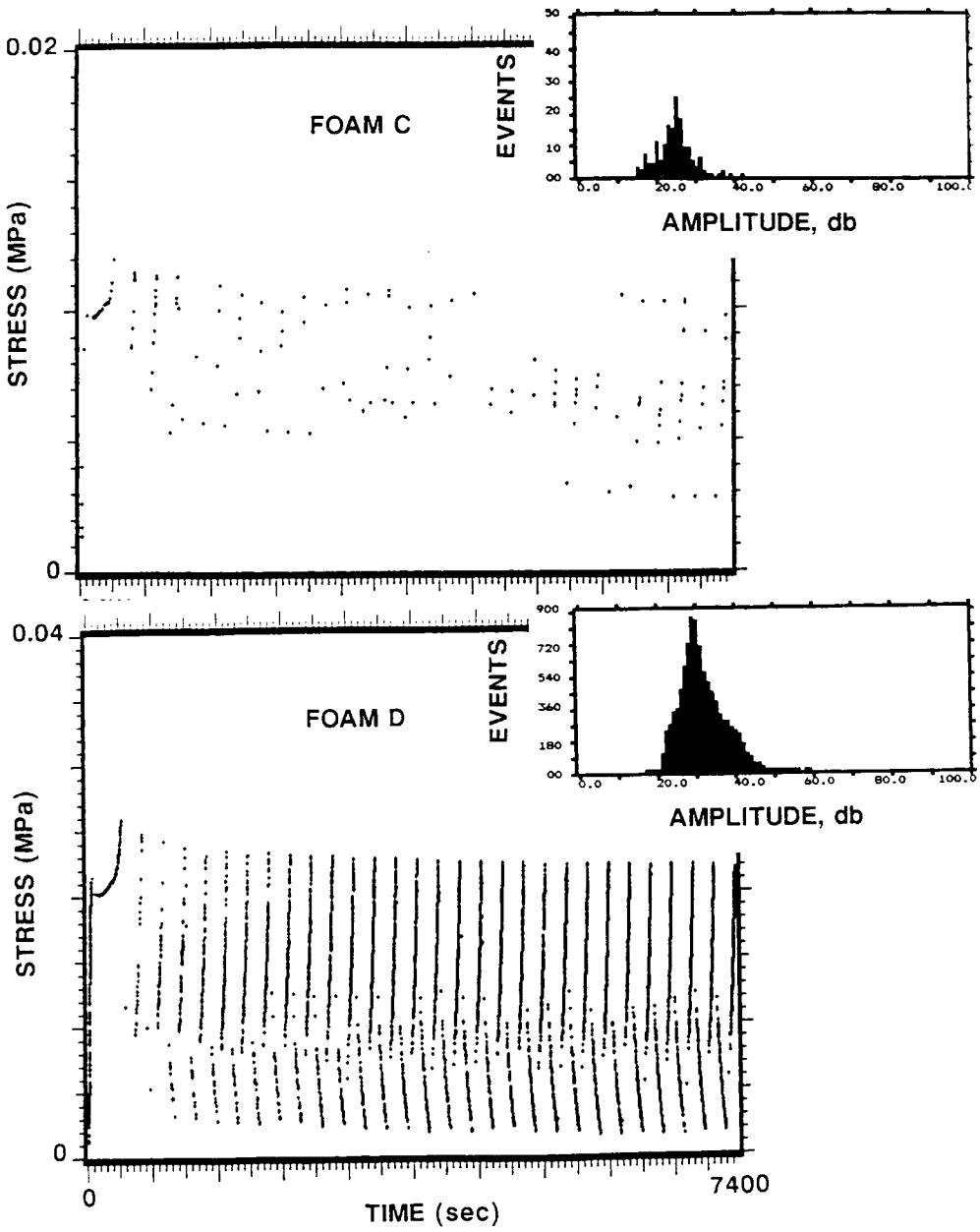

Figure 6 The AE activity of foams C and D during the first 30 cycles of compressive cycling.

age accumulated in foam C. The total amount of AE activity generated during 1000 cycles of compressive loading is shown in Figure 7. The histograms represent the number of AE events that occurred with time or cycle. In foam C, the AE activity rate increases gradually in the early cycles and stabilizes after about the 300th cycle. However, foam D has a rapid increase of the AE event rate up to about the 50th cycle and then levels off, reaching approximately the same amount of AE activity as in foam C after the 300th cycle. The significant difference of AE activity in the first 300 cycles between foams C and D during compressive cycling corresponds to the loss of the respective mechanical properties. This suggests that the irreversible damage occurring during fatigue loading leads to the decrease of the load-bearing capacity in these foams. The presence of more SAN particles results in both a higher modulus and a plateau stress; however, the higher content of this SAN copolymer also leads to more severe ir-

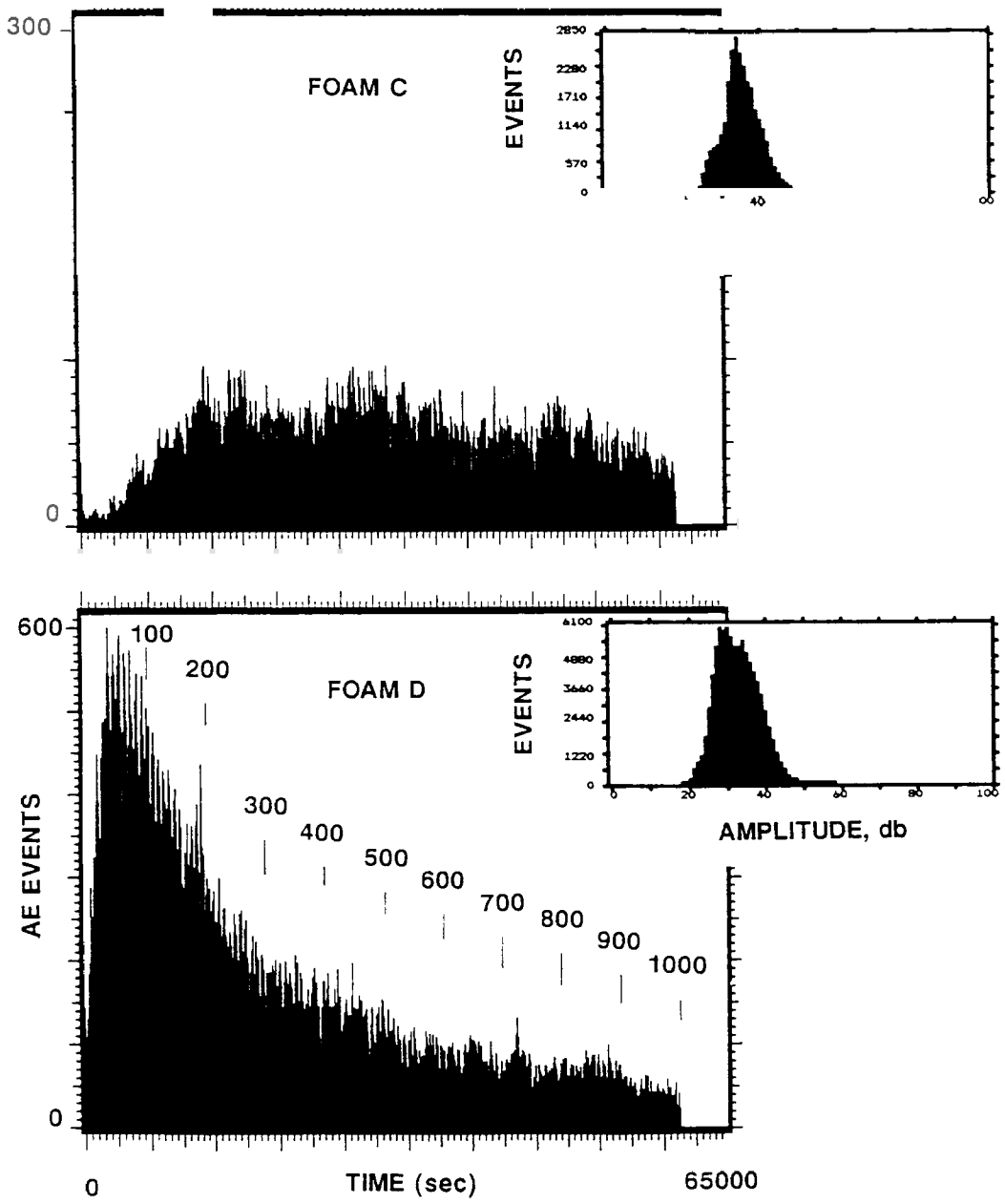

reversible damage and a subsequent greater decrease in the overall load-bearing capacity.

The amplitude distributions of AE events have been successfully utilized to identify the damage mechanisms in other heterophase polymeric systems.[24-27] A single peak amplitude distribution generally implies that one damage mechanism dominates. This is the case shown at the top right of Figure 7(a) and (b), indicating that both foams have the same damage mechanism with a peak around 32 db. For more detail analysis of these distributions, the amplitude distributions for each region for both foams are shown in Figures 8 and 9. Again, in all instances, there is only one peak and no change in amplitude distribution in both loading and unloading of foams C and D as cycling progressed. This suggests that only one damage mechanism dominates in all cases. Table II lists the average number

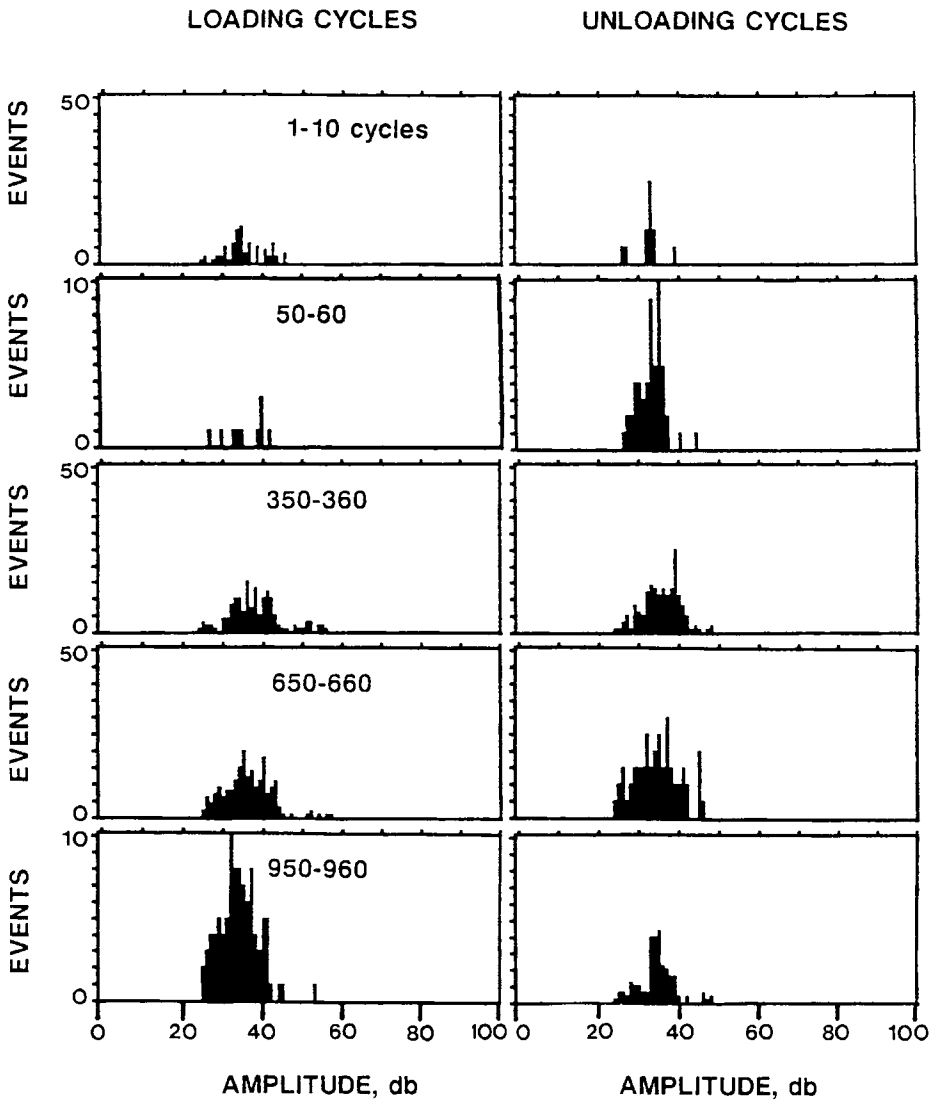

Figure 8 Amplitude distribution of AE events in foam C during cyclic loading.

of AE events per cycle in each region. Also, a considerable amount of AE activity generated during the unloading part of the cycle in both foams suggests that during the unloading friction between struts could cause both AE and additional irreversible damage.

2. *In Situ* SEM Observations

Based on the AE results obtained in cyclic compressive loading (Fig. 7), the maximum damage rate in foam D was observed around the 50th cycle. Therefore, similar cyclic loading conditions were simulated in the SEM and observations were recorded at the first and 51st cycles to determine the damage progression and to compare the effects of SAN particles on the visible irreversible damage. Figure 10 shows SEM photographs of foam C at 75% compression at the first and 51st cycles. The strut at the right side collapsed after 50 cycles of compressive loading. Higher magnification of these photographs are shown in Figure 11, where microcrazing is already observed in the first cycle. The size and density of microcrazes virtually did not change after 50 cycles. This may explain why there was little AE activity in foam C during the early stage of fatigue loading. High-magnification SEM photographs of a buckled strut in foam D on the first and 51st cycles are shown in Figure 12. Similar to foam C, after the first cycle, microcrazes occurred

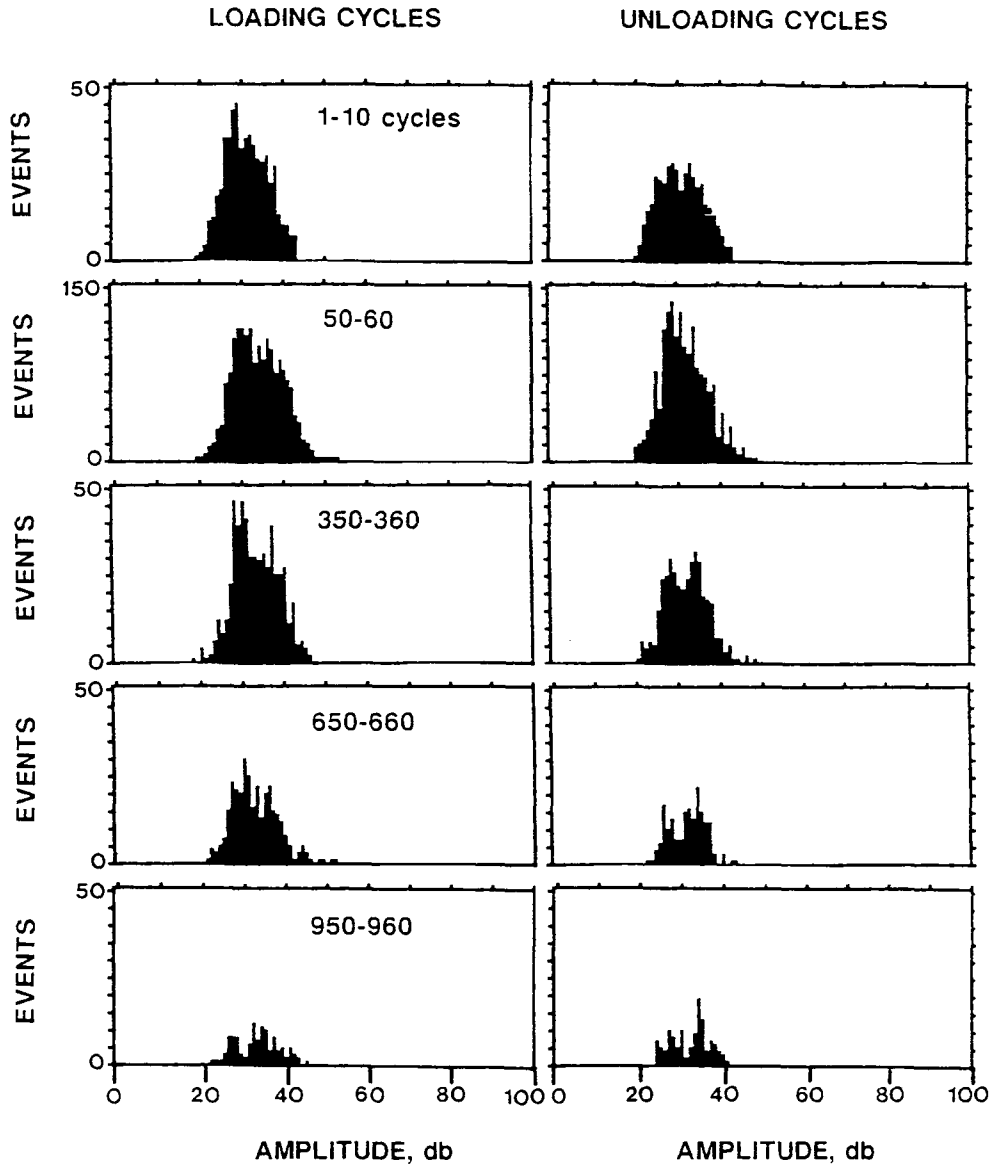

Figure 9 Amplitude distribution of AE events in foam D during cyclic loading.

in the struts. However, in this foam, the irreversible damage became much more severe as cycling progressed. These SEM observations reveal the damage processes in the struts of these SAN particle-reinforced flexible PU foams and supports the results from AE monitoring and from the cyclic mechanical tests. The presence of SAN particles produces sites for localized stress concentration, seemingly leading to irreversible profuse microcrazing. The higher content of SAN copolymer particles in foam D causes more severe irreversible damage, which is reflected in the larger amount of AE activity and the greater loss in load-bearing capacity.

IV. CONCLUSIONS

Acoustic emission (AE), which monitors the real-time damage progression as well as identifies the damage mechanisms, and *in situ* scanning electron microscopy, which sees the damage evolution, have been utilized to investigate the damage processes in SAN copolymer flexible PU foams. The presence of SAN particles increases the modulus and the plateau stress; however, these particles create the sites of localized stress concentration that lead to severe irreversible microcrazing, causing the reduction of the load-bearing capacity in fatigue. AE monitoring de-

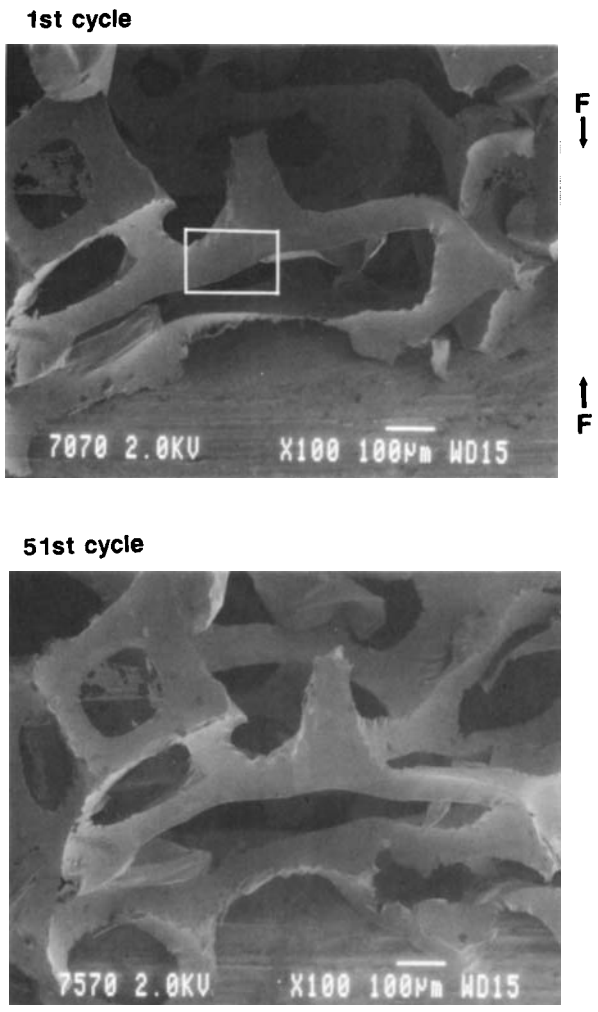

Figure 10 SEM photographs of foam C at 75% compression on the first and 51st cycles.

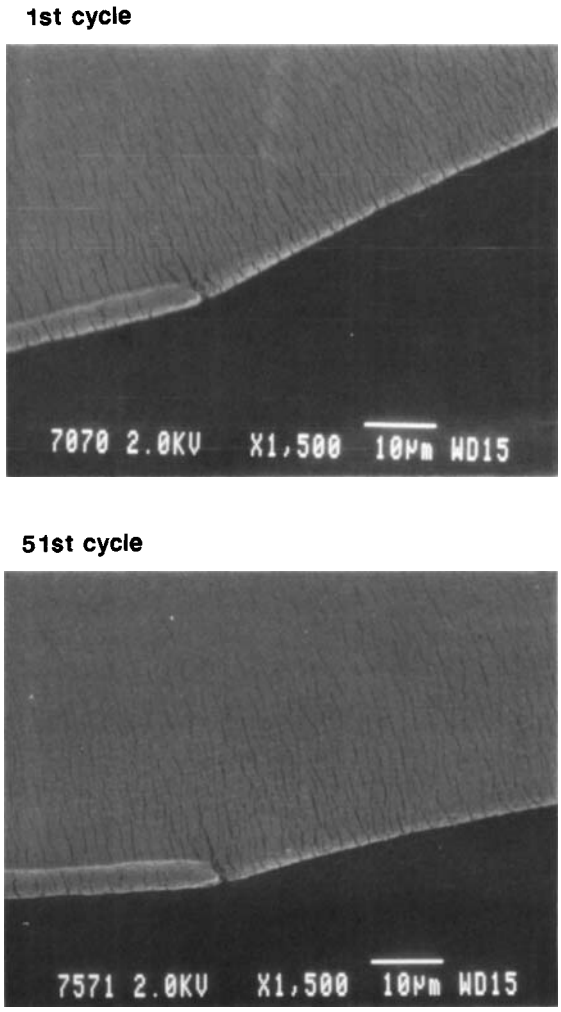

Figure 11 Higher magnification of Figure 10 showing the microcrazing in the cell strut.

Table II Average AE Events per Cycle in Each Region during 1000 Cycles Compressive Loading

	Foam C		Foam D	
Cycle	Loading	Unloading	Loading	Unloading
1–10	8	8	55	40
50–60	2	6	179	112
150–160	12	15	124	64
250–260	22	19	68	48
350–360	15	17	55	38
450–460	30	16	40	30
550–560	22	10	26	19
650–660	20	6	32	18
750–760	19	8	20	12
850–860	22	11	21	20
950–960	10	14	12	11

1st cycle

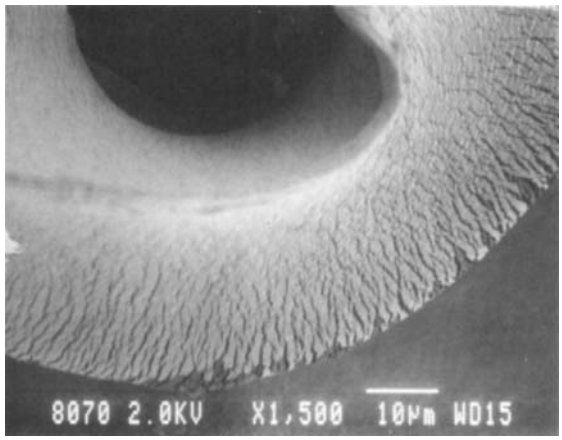

51st cycle

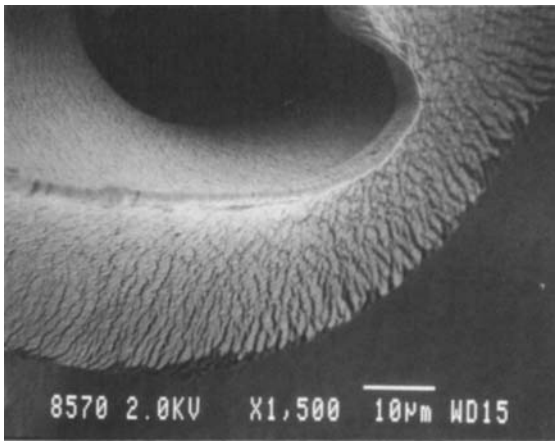

Figure 12 SEM photographs of foam D at 75% compression on the first and 51st cycles.

tected the extent of irreversible damage that corresponded to the loss of mechanical properties during fatigue loading. SEM observations reveal that microcrazing occurred during cyclic compression and was severe when high concentrations of SAN particles were used. It is suggested that the observed loss in mechanical properties in these foams and the large amount of AE activity observed during fatigue is due to microcrazing.

The authors wish to thank the Dow Chemical Company, Freeport, Texas, for their financial support of this work.

REFERENCES

1. W. I. Ko, *J. Cell. Plast.*, **1,** 45 (1965).
2. A. N. Gent and A. G. Thomas, *J. Appl. Polym. Sci.*, **1**(1), 107 (1959).
3. J. M. Lederman, *J. Appl. Polym. Sci.*, **15,** 693 (1971).
4. K. C. Rusch, *J. Appl. Polym. Sci.*, **13,** 2297 (1969).
5. S. K. Maiti, L. J. Gibson, and M. F. Ashby, *Acta Metall.*, **32**(11), 1963 (1984).
6. A. T. Huber and L. J. Gibson, *J. Mater. Sci.*, **23,** 3031 (1988).
7. P. E. Kreter, *J. Cell. Plast.*, **21,** 306 (1985).
8. A. L. Layter and A. C. Smith, *J. Mater. Sci.*, **23,** 736 (1988).
9. S. V. Kanakkanatt, *J. Cell. Plast.*, **9,** 50 (1973).
10. T. E. Neet, *J. Cell. Plast.*, **11,** 45 (1975).
11. E. T. Lloyd and G. M. Grays, *J. Cell. Plast.*, **15,** 47 (1979).
12. L. F. Lawler, Y. Televantos, and G. Combs, *J. Cell. Plast.*, **25,** 231 (1989).
13. Z. Korzeniowski and K. Piekarski, *J. Cell. Plast.*, **11,** 37 (1975).
14. R. B. Turner and G. L. Wilkes, in *Structure vs. Properties of Flexible Urethane Foams Used in the Home Furnishing Industry (Polymer–Morphology),* Kurt Frisch Symposium, University of Detroit, Detroit, IL, January 1988.
15. B. N. Stevens, J. F. Scott, D. J. Burchell, and F. O. Baskent, *J. Cell. Plast.*, **26,** 19 (1990).
16. H. Stone, *J. Cell. Plast.*, **19,** 47 (1983).
17. W. A. Ashe and O. M. Grace, *J. Cell. Plast.*, **25,** 371 (1989).
18. C. G. Seefried, Jr., R. D. Whitman, and D. F. Pollart, *J. Cell. Plast.*, **10,** 171 (1974).
19. B. Beals, F. J. Dwyer, and M. Kaplan, *J. Cell. Plast.*, **1,** 32 (1965).
20. F. J. Dwyer, *J. Cell. Plast.*, **12,** 104 (1976).
21. R. P. Kane, *J. Cell. Plast.*, **1,** 217 (1965).
22. W. M. Lee, *J. Cell. Plast.*, **20,** 369 (1984).
23. C. Kau, L. Huber, A. Hiltner, and E. Baer, *J. Rein. Plast. Comp.*, **8,** 18 (1989).
24. T. Weng, A. Hiltner, and E. Baer, *J. Mater. Sci.*, **21,** 744 (1986).
25. Yuan, A. Hiltner, E. Baer, and D. Rahrig, *J. Mater. Sci.*, **20,** 4377 (1985).
26. M. Faudree, A. Hiltner, E. Baer, and J. Collister, *J. Comp. Mater.*, **22,** 1170 (1988).

Received June 4, 1991
Accepted June 25, 1991